applied sciences

MDPI

Article

Experimental Investigation and Optimization of a Glazed Transpired Solar Collector

Catalin Ioan Teodosiu [1,*], Catalin Sima [1], Cristiana Croitoru [1] and Florin Bode [1,2]

[1] CAMBI Research Center, Technical University of Civil Engineering Bucharest, 021414 Bucharest, Romania
[2] Department of Mechanical Engineering, Technical University of Cluj-Napoca, 400020 Cluj-Napoca, Romania
* Correspondence: catalin.teodosiu@utcb.ro

Featured Application: Evaluation of energy saving for implementation of optimized glazed transpired solar collectors within the façades of buildings.

Abstract: Solar air collectors are increasingly used nowadays due to their important potential in reducing the energy consumption of buildings. In this context, glazed transpired solar collectors (GTCs) represent an interesting solution, but this type of solar air collector is less studied. Consequently, the objective of this work is to thoroughly assess the performance of a GTC prototype under real long-term climatic conditions. First, the design of the GTC is optimized based on methodically experimental tests. The results show that the GTC configuration with a 30 mm air gap among the absorber and the glazing leads to improved heat transfer efficiency and superior global effectiveness, regardless of airflow rates through the solar air collector. This optimized GTC configuration is further studied by integration within the façade of a full-scale experimental building (container-type, light structure). Comparative experimental studies are then carried out concerning the heating energy consumption and ventilation load of the experimental building without/with GTC implemented in the ventilation system, under Bucharest real weather conditions. The data achieved indicate that the GTC prototype is capable of substantially reducing the ventilation load: up to 25% for low solar radiation (below 200 W/m^2) and over 50% (achieving even 90%) for moderate solar radiation (between 250 and 380 W/m^2). Finally, for high solar radiation (over 400 W/m^2), the GTC outlet air temperature exceeds the interior temperature set-point (22 °C) of the experimental building.

Keywords: glazed transpired solar collectors (GTC); building ventilation; experimental measurements

Citation: Teodosiu, C.I.; Sima, C.; Croitoru, C.; Bode, F. Experimental Investigation and Optimization of a Glazed Transpired Solar Collector. *Appl. Sci.* **2022**, *12*, 11392. https://doi.org/10.3390/app122211392

Academic Editor: Andrea Frazzica

Received: 19 October 2022
Accepted: 7 November 2022
Published: 10 November 2022

1. Introduction

In the present-day (tense) context related to the energy crisis, the European Commission recently proposed a series of exceptional measures to tackle this issue [1]. Logically, the first and most important action nowadays is to reduce energy demand, according to the axiom: "the cheapest energy is the one you don't use". On the other hand, the European Union (EU) had set impressive goals concerning the renewable share of its gross final energy consumption, 20% by 2020 [2], increasing to 32% by 2030 [3]. According to European Environment Agency (EEA) estimations, renewable sources supplied 22% of the EU energy consumption in 2021 [4]. Sector-level analysis shows that renewable energy sources (RES) represented almost 38% of all electricity produced across the EU in 2021 [4]. This increased RES contribution in the power sector leads to new challenges in the near future: the need for models for accurate and reliable forecasting macro-area power generation [5]—including energy efficiency indicators taking into account the renewable share [6] and cost analysis for energy systems with a high share of renewable energy (over 70%) [7]; the requirement of new policies and governance instrument frameworks for the electricity market [8]; impact studies related to support schemes for renewables on electricity markets [9]; and environmental analysis for the evaluation, comparison, and selection of energy supply systems based on new parameters (e.g., expanded total equivalent warming impact [10]).

Furthermore, the heating and cooling of buildings in the EU benefitted from the greatest growth RES share (reaching 23.6%) in 2021 [4]. In this context, it is worth mentioning that buildings and the construction sector are still responsible for 36% of the global final energy consumption and 37% of energy-related CO_2 emissions in 2021 [11]. These figures explain the major interest regarding the implementation of energy efficiency solutions and the usage of RES in the building sector. Concerning the RES for heating and domestic hot water, the latest data show that the solar thermal market witnessed a 3% growth in 2021 after seven years of market declines [12]. This increase corresponds to the following numbers (at the end of 2021): 746 million square meters of collector area; 522 GW—cumulated capacity in operation; and 425 TWh energy produced per year (2021), meaning savings of 45.7 million tons of oil and 147.5 million tons of CO_2 [12]. Certainly, most of the solar thermal applications are based on solar water collectors. Nevertheless, solar air systems almost reached 1.5 million square meters of collectors' area (glazed and unglazed air collectors) in operation worldwide—nearly 1 GW installed capacity by the end of 2020 [12].

This expansion of solar air collectors is mainly explained by the following considerations: no risk of frost [13], cost-effective solution [14], supply of high-temperature air [15], high potential in reducing the energy consumption of buildings [16], multiple applications (e.g., space heating [17,18], preheating of fresh air—ventilation [19], and the drying agricultural food products [20]), and reduced operating costs [16].

On the other hand, solar air-heating technology is based on several types of solar collectors: bare plate, back-pass, glazed, unglazed, covered, uncovered, perforated, unperforated, single pass, double pass, etc. [21]. In addition, numerous modifications have been investigated to improve the performance of all these types of solar air collectors [22]: modified absorber plate (e.g., sinusoidal corrugations on absorber plate, curved absorber plate, and arched absorber plate with equilateral triangular turbulator and dimply turbulator); integration of a porous medium (e.g., wire mesh and metal scraps); and the implementation of energy storage solutions (e.g., phase-changing materials and plastics).

Among these types and improved models of solar air collectors, the ones with a perforated absorber element (called "Transpired Solar Collectors"—TSCs) have been analyzed for almost 40 years [23]. Studies have shown that the heat lost through convection and radiation at the surface of the plate can be recovered by manufacturing perforations in the absorber, as in the case of TSCs [24,25]. Consequently, compared to unperforated (flat absorber element) solar collectors, TSCs are 28–50% more efficient under the same climate conditions [25,26]. Therefore, TSCs have been successfully employed in buildings [16,18,27]. For instance, the use of TSCs for fresh air heating has led to excellent results: more than 70% efficiency [19] and almost 75% energy saving [28]. In addition, according to Li et al. [29], the use of TSCs has resulted in the best performances for school classroom ventilation in winter, considering energy saving, environmental protection, and economic impact, compared to other solutions for air heating (air conditioners or electric heaters). Tajdaran et al. [30] also revealed that TSCs represent interesting solutions for regions with reduced solar radiation.

On the other hand, the efficiency of TSCs is strongly influenced by the wind [19]. Cordeau and Barrington [24] experimentally investigated the performance of TSCs depending on the wind. The results revealed that the TSC average efficiency is 65% for wind velocities below 2 m/s but the TSC average efficiency decreases below 25% for wind velocities above 7 m/s. These results have been confirmed by computational fluid dynamics simulations dealing with TSCs: a wind velocity between 0.5 and 2 m/s would not have such a great impact on the TSCs' heat transfer effectiveness, but for wind velocities exceeding these values, the TSCs' efficiency would considerably decrease [31]. Furthermore, Konttinen et al. [32] thoroughly studied the degradation over time due to meteorological factors (e.g., acid and neutral rain) of aluminum absorber elements in the case of TSCs. Their results showed that the degradations of absorber optical properties (e.g., emittance) are important if the TSCs are exposed to rain with a pH exceeding 3.5–4.5. Therefore, this type of solar air collector is not recommended to be used in such operating conditions. In addition, the façade of the building could be degraded due to water infiltration through the perforations of the absorber.

In order to cope with these problems related to weather conditions (wind, rain, and snow), the TSCs can be provided with a layer of glass applied to the surface of the absorber plate. This type of solar air collector is known as "Glazed Transpired Solar Collector"—GTC. Comparisons carried out between TSCs and GTCs highlighted better performances for GTCs, particularly for applications in cold climates: the annual solar fraction for air-heating systems based on GTCs is nearly nine times higher than that based on unglazed transpired collectors (TSCs) in the severe cold climate region of China [33]; the thermal performance and economic characteristics of GTCs with a perforated corrugated plate are superior in comparison with other types of TSCs in rural areas of cold regions [34]; the heat loss of GTCs can be reduced up to 40% compared to TSCs in the case of powerful wind and cold zones [35]; and GTCs could also lead to improved indoor environments [36].

Despite these significant accomplishments, GTC design optimization is essential to keep on improving the heat exchange rate. For instance, Nahar and Garg [37] proposed an air layer of 40 to 50 mm between the absorber plate and the cover glazing in order to minimize both shading and heat losses through convection. Charvat et al. [38] have analyzed the thermal performance of glazed solar air collectors without/with phase change material (an absorber plate of simple sheet metal/an absorber plate containing nine aluminum containers filled with paraffin) under real climatic conditions. They concluded that the configuration with thermal storage integrated in the absorber led to better efficiency and higher stability of the collector outlet air temperature. In addition, there are many studies focusing on the optimization of the GTC absorber. Three types of GTC absorber were considered for comparison by Karim and Hawlader [39] over a wide range of operating and design conditions: flat plate, finned plate, and v-corrugated plate. Their data showed that the v-corrugated absorber was the most efficient while the flat absorber was the least efficient, regardless of configuration (single pass or double pass). El-Sebaii et al. [40,41] also compared two configurations of an absorber made of copper: double-pass finned plate and double-pass v-corrugated plate. The results confirmed, based both on theoretical and experimental analyses, that the GTC with the v-corrugated plate was roughly 10–14% more efficient. Chabane et al. [42] found that longitudinal fins attached behind the GTC absorber plate improved the heat exchange, with the efficiency being increased by 5–7.5% (depending on the airflow rate) for the configuration with fins compared to that without fins. Ozgen et al. [43] investigated the possibility to enhance the GTC efficiency by using an absorber made of aluminum cans. The best efficiency was achieved for the configuration with the aluminum cans positioned in a zigzag pattern on the absorber. Moreover, the results achieved by Omojaro and Aldabbagh [44] pointed out that using steel wire mesh arranged in layers as an absorber for the GTC led to a significant rise in thermal efficiency. Similar results have been reported by El-khawajah et al. [45], based on a comparable design (wire mesh layers used between fins as a replacement for the absorber), reaching a maximum efficiency up to almost 86%. Finally, Gao et al. [46] studied a new design of a GTC with a perforated corrugated plate, having both an air inlet and air outlet at the bottom of the solar air collector. The results showed that this different airflow path within the GTC was capable of improving the heat exchange efficiency by almost 20%, compared to the conventional solution (an air inlet at the bottom and the air outlet at the top of the solar air collector).

Despite the aforementioned studies, it is still necessary to deepen the research concerning GTCs' optimization and to assess GTCs' performance under varying weather and operating conditions. In this context, the aim of this study is to thoroughly evaluate the performance of GTCs in the conditions of Romania's cold climate. As a result, experimental investigations have been carried out using a GTC prototype. The experimental study has included two main stages: a preliminary work regarding the optimization of the GTC configuration, followed by a long-term performance analysis of the optimized GTC, integrated in the façade of a building, under real climate conditions. Each of these two parts of the experimental study is presented in detail below, including comprehensive analyses and a discussion of the results.

2. Materials and Methods

First, it is worth mentioning that this work was carried out in the frame of recent activities fulfilled by the CAMBI Research Center, concerning solar air collectors: innovative unglazed TSCs based on absorbers with lobed cross-shaped perforations [47], TSCs with phase change materials [48,49], and double-skin transpired solar collectors (DSTSCs) [50]. Consequently, the construction of the GTC prototype was based on one of the existing TSC models within the CAMBI Research Center [51], adding the glass cover plate to reduce the convective heat loss due to wind and to assess the behavior of the resulting GTC configuration under the conditions of the cold climate of Romania. The GTC experimental set-up, with all the implemented enhancements, is detailed further down.

2.1. Optimization of the GTC Design

2.1.1. Experimental Set-Up and Protocol

The GTC configuration considered is presented in Figure 1. The working principle of this GTC is almost identical to that of TSCs. The air is supplied to the bottom part (see Figure 1), passing both through the cavity between the glass layer and the absorber plate and through the orifices of the absorber plate. Finally, the heated air is collected at the top of the GTC, in a plenum, and then extracted through a circular duct (160 mm) by a variable-speed fan (type EBM-Papst).

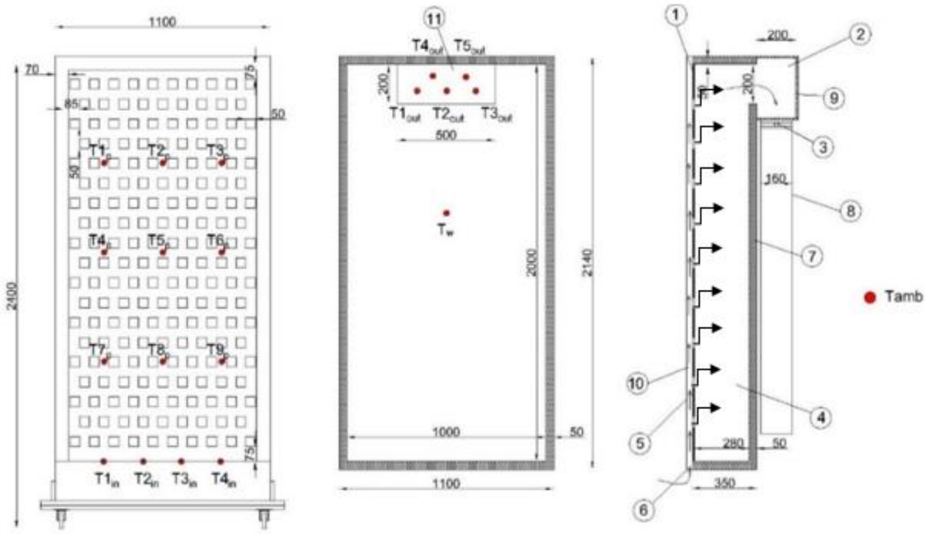

Figure 1. GTC design details: 1—transpired steel plate; 2—plenum; 3—fan; 4—inner cavity; 5—glazing; 6—air inlet; 7,9—thermal insulation; 8—air duct; 10—air layer between glass and absorber; 11—air outlet.

The frame of the GTC was built of the following materials: a wooden structure and OSB (oriented strand board) plates. The space between the OSB plates was filled with thermal insulation—rock wool (thickness of 50 mm). The GTC absorber (2000 mm × 1050 mm) was made of a steel plate (thickness of 2 mm), painted black. On the other hand, the main change in the GTC design, compared to previous solar air collectors analyzed at the CAMBI Research Center, was related to the perforations of the absorber. The size, shape, and pitch of the absorber perforations could be important influence factors on the efficiency of transpired solar collectors [52]. Van Decker et al. [53] reported that about 28% of the air's heat gain is due to the plate perforations. On the other hand, Gao et al. [33] determined, based on experimental data, that the solar collector efficiency is not significantly influenced by reducing the dimensions of the absorber perforations (only a 0.56% increase for decreasing the diameter of the perforations from 20 mm to 10 mm). Consequently, the new proposed design of the GTC was based on larger and simpler perforations (50 × 50 mm) uniformly distributed on the absorber plate (Figure 2). This allows considerably simplifying the manufacture of the GTC and obtaining a low-cost solar air collector model. It is worthwhile to mention that this simplified absorber configuration of the GTC prototype represents one of the major novelties of this study because more complicated absorber solutions (both regarding the perforations and their arrangement) are usually investigated in the literature, as shown above. Consequently, the study of this basic configuration is even more interesting to be able to determine if it allows obtaining satisfactory results.

Figure 2. GTC picture with square perforations on the absorber plate.

Normal window glass (thickness of 4 mm) was used as the glazing for the GTC (Figure 2). This GTC glazing cover can be mounted, due to the experimental set-up configuration, at variable distances from the absorber plate (30, 50, 70, or 90 mm).

Finally, the entire GTC structure was painted in black, using ordinary paint (Figure 2).

The different measurements of temperatures within the experimental set-up are carried out using 19 K-type thermocouples (Figure 1):

- 4 thermocouples on the air GTC inlet ($T_{1–4\ in}$);
- 5 thermocouples on the air GTC outlet ($T_{1–5\ out}$);
- 9 thermocouples on the GTC absorber plate ($T_{1–9p}$);
- 1 thermocouple on the inner surface of the GTC rear wall (T_w).

It is worth mentioning that before performing the experimental study and starting the measurements, all temperature sensors mentioned above were calibrated using a thermostatic bath (Lauda RE 1225 S).

A flow meter (FlowFinder mk2) was used to determine the airflow through the GTC. The installation of the flow meter is shown in Figure 3. This set-up allows precise and reliable airflow measurements.

Figure 3. Flow meter installation within the experimental set-up.

In addition, meteorological data were logged during the GTC experimental study. Ambient temperature, solar radiation intensity, and wind speed and direction were recorded using the Almemo weather station with different sensors, positioned at the top of the GTC (Figure 2).

The main features of all measuring instruments used in this study are presented in Table 1.

Table 1. Measuring devices' characteristics.

Instrument	Type	Parameter	Range	Uncertainty
Thermocouple	K (NiCr-Ni)	Temperature	$-10\ldots+105$ °C	±0.2 °C
Air flow meter	FlowFinder mk2	Air flow	$10\ldots550$ m^3/h	3%
Digital sensor	Almemo FHAD 46-C2	Ambient temperature	$-20\ldots+60$ °C	±0.2 °C
Cup-type anemometer	Almemo FVA 615 2	Wind velocity	$0.5\ldots50$ m/s	3%
Wind vane	Almemo FVA 614	Wind direction	$0\ldots360°$	±5°
Star pyranometer	Almemo FLA 628 S	Solar radiation intensity	$0\ldots1500$ W/m^2	<3%

All the experimental data were acquired by means of 2 × Almemo 710 data loggers, with the recording step being 30 s.

Two GTC designs were considered, with different distances between the absorber plate and the glass layer, 30 mm and 50 mm, respectively. The air flow rates were, for each of these two configurations: 150, 200, 250, 300, 350, and 400 m^3/h.

The experimental study was carried out in the second part of October 2019. The measurements were accomplished every day between 12:00 and 18:00.

2.1.2. Results and Discussion

- Meteorological data:

The GTC experimental stand is located in the courtyard of the CAMBI Research Center laboratory, within the premises of the Faculty of Building Services Engineering—Technical University of Civil Engineering Bucharest. We present below the weather data for this location (66, Pache Protopopescu Boulevard—Bucharest: 44°26′22.8″ N 26°07′33.6″ E), recorded during the experimental studies. It should be noted that the reported data (Tables 2 and 3) represent average values during the interval 13:10–14:10 for each day of measurements (one day of experimental study corresponds to an air flow rate value for each configuration, 30 mm or 50 mm distance between the absorber and the glazing).

Table 2. GTC configuration: 30 mm-distance absorber—glazing. Mean values of meteorological parameters (time interval: 13:10–14:10).

Parameter/Day (Airflow Rate)	11 October ($158\ m^3/h$)	12 October ($203\ m^3/h$)	13 October ($250\ m^3/h$)	14 October ($296\ m^3/h$)	15 October ($354\ m^3/h$)	16 October ($397\ m^3/h$)
Ambient temperature (°C)	26.5	25.2	28.1	28.4	21.5	21.8
Solar radiation intensity (W/m^2)	770.7	785.8	758.9	719.4	771.0	755.7
Wind velocity (m/s)	0.32	0.46	0.35	0.17	0.13	0.15

Table 3. GTC configuration: 50 mm-distance absorber—glazing. Mean values of meteorological parameters (time interval: 13:10–14:10) [1].

Parameter/Day (Airflow Rate)	18 October ($154\ m^3/h$)	19 October ($205\ m^3/h$)	20 October ($254\ m^3/h$)	21 October ($302\ m^3/h$)	23 October ($350\ m^3/h$)
Ambient temperature (°C)	22.6	25.1	23.7	28.4	22.8
Solar radiation intensity (W/m^2)	681.9	659.7	685.6	684.5	617.8
Wind velocity (m/s)	0.21	0.16	0.11	0.12	0.27

[1] experimental data only for 5 days (5 airflow rates) for the reason of unfavorable weather conditions recorded on the measurement day for the airflow rate of 400 m^3/h.

This same study period (13:10–14:10) for each day was chosen because the solar radiation and outdoor air temperature have relatively constant values during all the days of the experimental study in this interval. In addition, the values of these climatic parameters are very close from one day to another in this interval (see Tables 2 and 3). This allows the exploitation and comparison of experimental results under relatively close weather conditions in order to obtain correct findings.

- GTC thermal behavior:

The GTC thermal behavior under different operating conditions can be evaluated by the following parameters: the difference between the GTC inlet air temperature and GTC outlet air temperature and the GTC absorber plate temperature. These data are presented in Tables 4 and 5 for each of the two GTC configurations considered.

Table 4. GTC configuration: 30 mm-distance absorber—glazing. GTC thermal parameters—mean values (time interval: 13:10–14:10).

Parameter/Day (Airflow Rate)	11 October ($158\ m^3/h$)	12 October ($203\ m^3/h$)	13 October ($250\ m^3/h$)	14 October ($296\ m^3/h$)	15 October ($354\ m^3/h$)	16 October ($397\ m^3/h$)
$\Delta T = T_{outlet} - T_{inlet}$ (°C)	18.1	13.9	13.4	12.6	11.2	10.2
Absorber plate temperature (°C)	57.8	54.6	53.3	48.7	41.5	39.5

Table 5. GTC configuration: 50 mm-distance absorber—glazing. GTC thermal parameters—mean values (time interval: 13:10–14:10) [2].

Parameter/Day (Airflow Rate)	18 October ($154\ m^3/h$)	19 October ($205\ m^3/h$)	20 October ($254\ m^3/h$)	21 October ($302\ m^3/h$)	23 October ($350\ m^3/h$)
$\Delta T = T_{outlet} - T_{inlet}$ (°C)	13.2	9.6	9.6	8.1	5.4
Absorber plate temperature (°C)	52.7	48.9	44.9	43.9	39.3

[2] experimental data only for 5 days (5 airflow rates) for the reason of unfavorable weather conditions recorded on the measurement day for the airflow rate of 400 m^3/h.

It can be noticed, based on the data from Tables 4 and 5, that both the air outlet–inlet difference temperature and the absorber temperature decreased linearly with the increase in the airflow through the GTC. This is valid for both analyzed configurations. On the other hand, the rise in temperature of the air passing through the GTC was roughly 4–5 °C higher in the case of the GTC configuration with 30 mm distance between the absorber and the glazing for the same values of airflow rates. This is due to the modified space between the absorber and the glass layer, but it must also be taken into account that the experimental tests for the GTC configuration with a 30 mm air gap among the absorber and the glazing benefited from more important solar radiation intensities and higher ambient air temperatures on some days. Nevertheless, Ferahta et al. [54] highlighted the same phenomenon: increased air layer thickness between the absorber and the glass affects the heat transfer within the solar collector due to an enhancement of heat losses through convection at the front (glazing) of the solar collector.

- GTC performance evaluation:

The heat transfer effectiveness of solar collectors can be evaluated using the following simplified calculation method [18]:

$$\varepsilon_{HX} = \frac{T_{outlet} - T_{ambient}}{T_{plate} - T_{ambient}} \tag{1}$$

where T_{outlet}—outlet air temperature (°C); $T_{ambient}$—ambient air temperature (°C); and T_{plate}—absorber plate temperature (°C).

Based on Equation (1), the variation in the heat exchange effectiveness with the airflow rate for the two GTC configurations is shown in Figure 4. It should be noted that the uncertainty in the derived results of GTC heat transfer effectiveness, based on measurement uncertainties (according to the values in Table 1), is around ±0.02. The uncertainty propagation calculation was performed using a deterministic method (differential error analysis) [55].

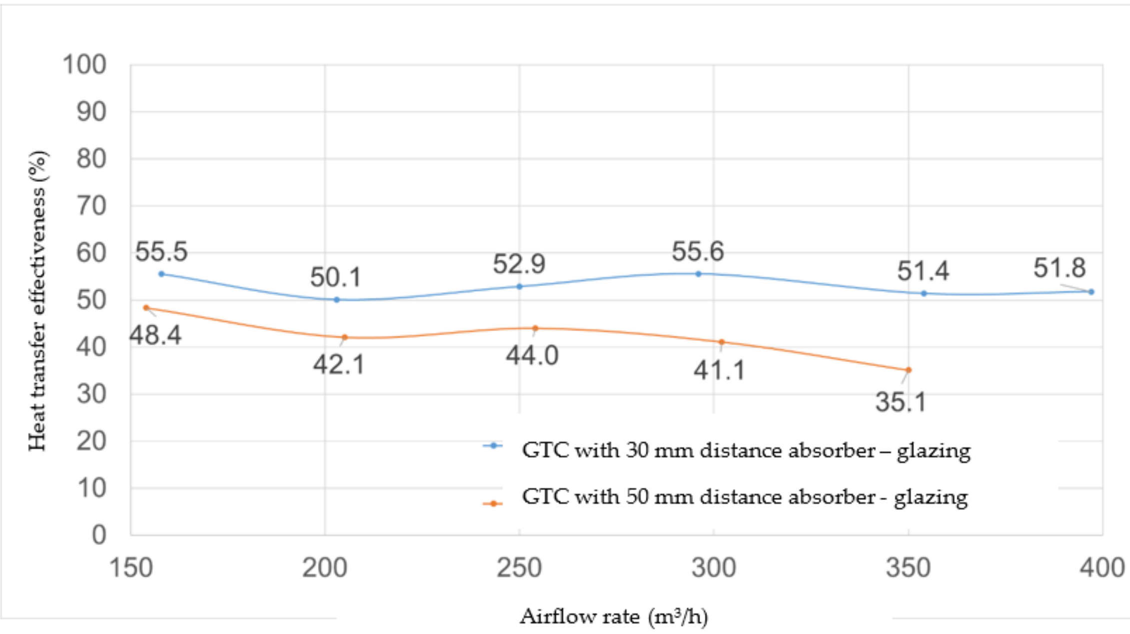

Figure 4. GTC heat transfer effectiveness.

It can be seen that the heat transfer efficiency within the GTC was superior in the case of the 30 mm distance between the absorber plate and the glass layer. Furthermore, for this configuration, the heat transfer effectiveness was constant, around 50–55%, regardless of the airflow rate through the solar collector.

The GTC performance can be also assessed by another criterium, related to the global efficiency of solar collectors [18]:

$$\eta = \frac{V\rho c_p(T_{outlet} - T_{ambient})}{I_T A_S} \tag{2}$$

where V—GTC airflow rate (m^3/s); ρ—air density (kg/m^3); c_p—air specific heat capacity (J/kg/°C); T_{outlet}—GTC outlet air temperature (°C); $T_{ambient}$—ambient air temperature (°C); I_T—total incident solar radiation on the GTC absorber (W/m^2); and A_S—GTC absorber area (m^2).

Figure 5 shows the variation in the GTC global efficiency with the airflow rate for the two considered configurations, according to Equation (2). The uncertainty in the final values of the GTC global efficiency resulting from the measurements' uncertainties was under ±0.5, based on the same method (differential error analysis).

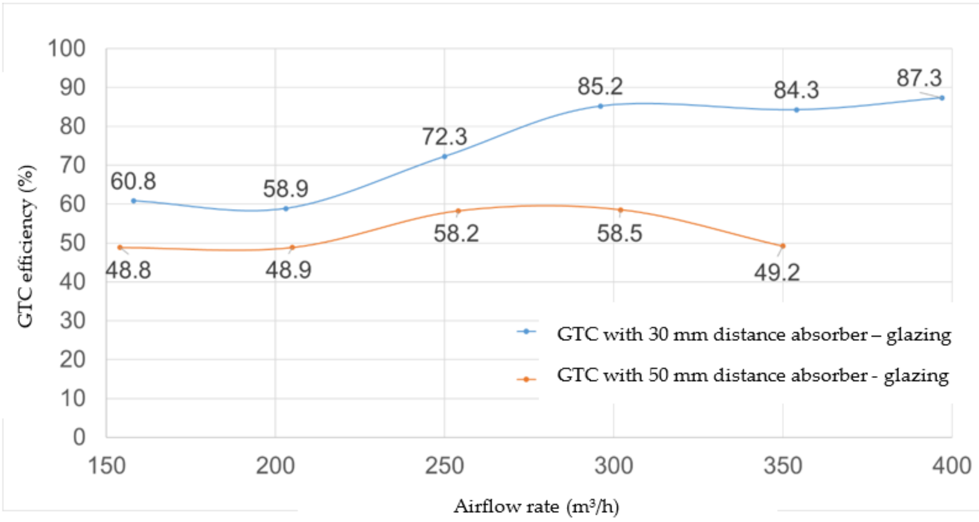

Figure 5. GTC global efficiency.

It can be observed that the GTC configuration based on reduced thickness of the air gap confined between the absorber and cover glazing was much more efficient, especially for higher airflow rates.

According to the above results, the GTC design with a distance of 30 mm between the absorber and the glass layer was more efficient than the GTC with a distance of 50 mm. Consequently, this GTC configuration with the air layer of 30 mm between the perforated plate and the glazing will be further studied by integration in the façade of a building. This study is presented further down.

2.2. Integration of the Optimized GTC into a Building Façade

2.2.1. Experimental Set-Up and Protocol

This second experimental study is performed by means of a full-scale experimental building, using a light container-type structure (6 m × 2.4 m × 2.5 m). The optimized GTC (with a distance between the perforated plate and the glass of 30 mm), according to the results presented above, is mounted on the façade of the container (Figure 6).

Figure 6. GTC on the façade of the experimental building.

This experimental set-up was also located near the CAMBI Research Center, within the premises of the Faculty of Building Services Engineering—Technical University of Civil Engineering Bucharest.

The container was characterized by low thermal inertia but with relatively good thermal insulation according to the data in Table 6.

Table 6. Thermal resistance—container envelope components.

Envelope Component	Thermal Resistance (m^2 °C/W)
wall	1.47
floor	0.30
roof	1.47
window	0.59
door	0.82
solar wall	1.33

The same type and number of measuring devices were mainly used as in the previous experimental study (see Table 1 and Figure 1). Their position was mostly the same, too (e.g., thermocouple's location within the GTC; see Figure 1). The sensors of the weather station were installed on the left corner of the container in order not to influence or obscure the measured parameters (Figure 7).

Figure 7. Installation of the weather station sensors on the container.

The data acquisition was achieved this time using a much larger storage memory data logger (Almemo 5690-2) to allow the monitoring over longer periods of time. The data logger and the fan power supply were installed in the container, next to the GTC (Figure 8).

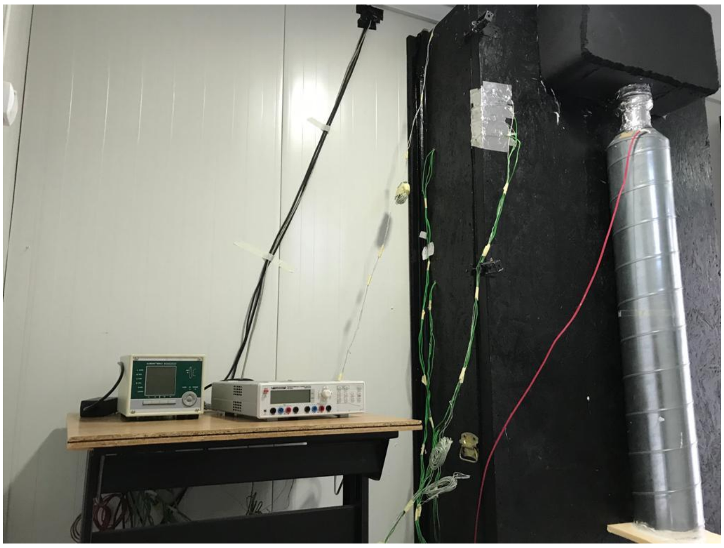

Figure 8. Installation of the data logger and the fan power supply in the container.

The experimental building was equipped with an air conditioning unit (2.6 kW capacity)—Figure 9. This equipment is used for the heating of the experimental building, operating in "air-to-air" heat pump mode.

Figure 9. Air conditioner.

A Strohm power meter socket was employed to record the energy consumption of the air conditioner during the experimental investigations (range: 1–3680 W; uncertainty: ±1%).

The value of the airflow rate through the GTC is correlated with the required fresh air of the experimental building. Consequently, the imposed airflow rate was 72 m^3/h, meaning 2 h^{-1} ACH (air changes per hour)—suggested outdoor air ventilation rate [56]. In order to achieve this low airflow rate, the GTC was equipped with an EBM-Papst 4184N/2X variable-speed fan and Rohde & Schwarz HMP2020 programmable power supply (output voltage 0–32 V DC; output voltage resolution 1 mV; voltage stabilization $\leq$ 0.01% + 2 mV;

output current 0-10 A; output current resolution 1 mA; and current stabilization $\leq$ 0.01% + 250 µA)—Figure 8.

The objective of the experimental study was to compare the energy consumption for ventilation of the experimental building (container) without/with a GTC. The measurements were performed in April–May 2021. It should be specified that no experimental investigations were conducted during rainy days.

Finally, in order to facilitate the comparisons, the GTC was completely covered by a white panel (with the exception of air intake) to study the configuration without the GTC (Figure 10). In this way, equivalent operating conditions were obtained for ventilation (the same airflow rate, pressure loss, and therefore, similar fan energy consumption).

Figure 10. Experimental set-up: configuration without GTC.

2.2.2. Results and Discussion

- Meteorological data:

We present below a sample of meteorological data recorded during the experimental campaign (Figure 11—intensity of the solar radiation and Figure 12—ambient temperature).

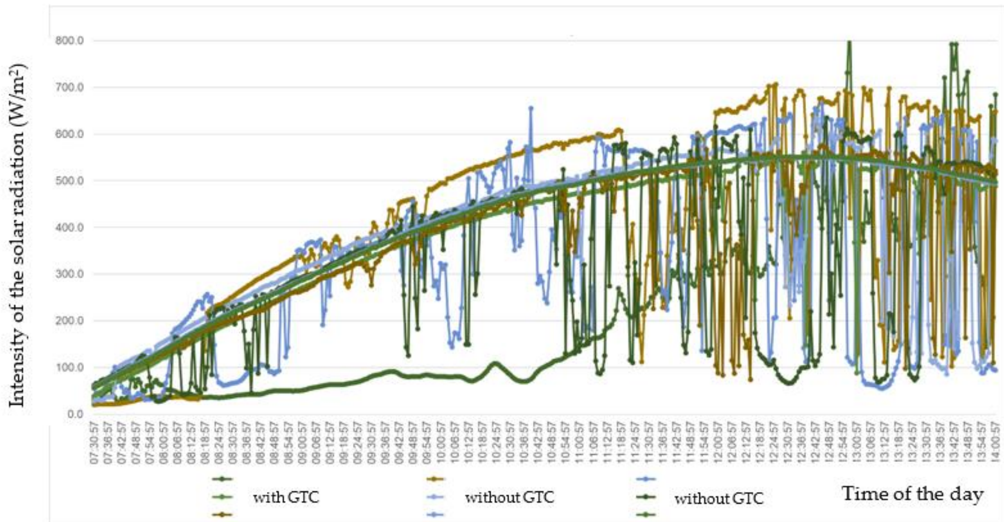

Figure 11. Solar radiation intensity for several days during the experimental tests.

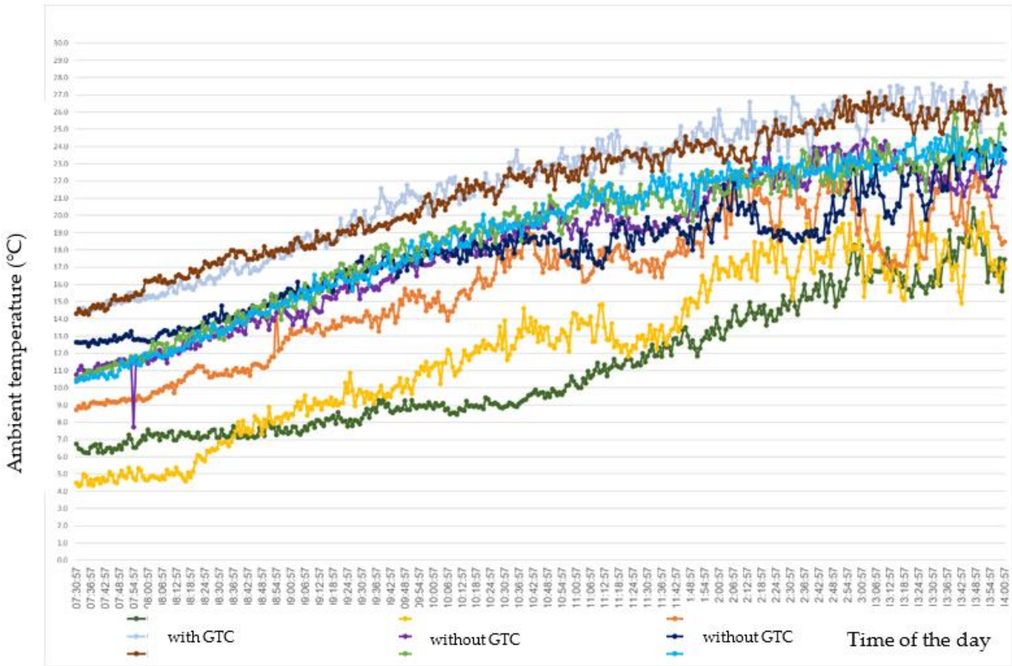

Figure 12. Outdoor temperature for several days during the experimental tests.

As can be seen, there were major discrepancies regarding the weather conditions for the days when the measurements took place.

For this reason, we selected for our analysis only the sequences of days with somewhat similar outside temperature and sunshine. For instance, one of the best such sequences for comparisons without/with a GTC is for the following days: 10 May 2021 and 11 May 2021 for the building without a GTC and 18 May 2021 for the building with a GTC. The diurnal variation in the solar radiation and air temperature for these days is shown in Figures 13 and 14, respectively.

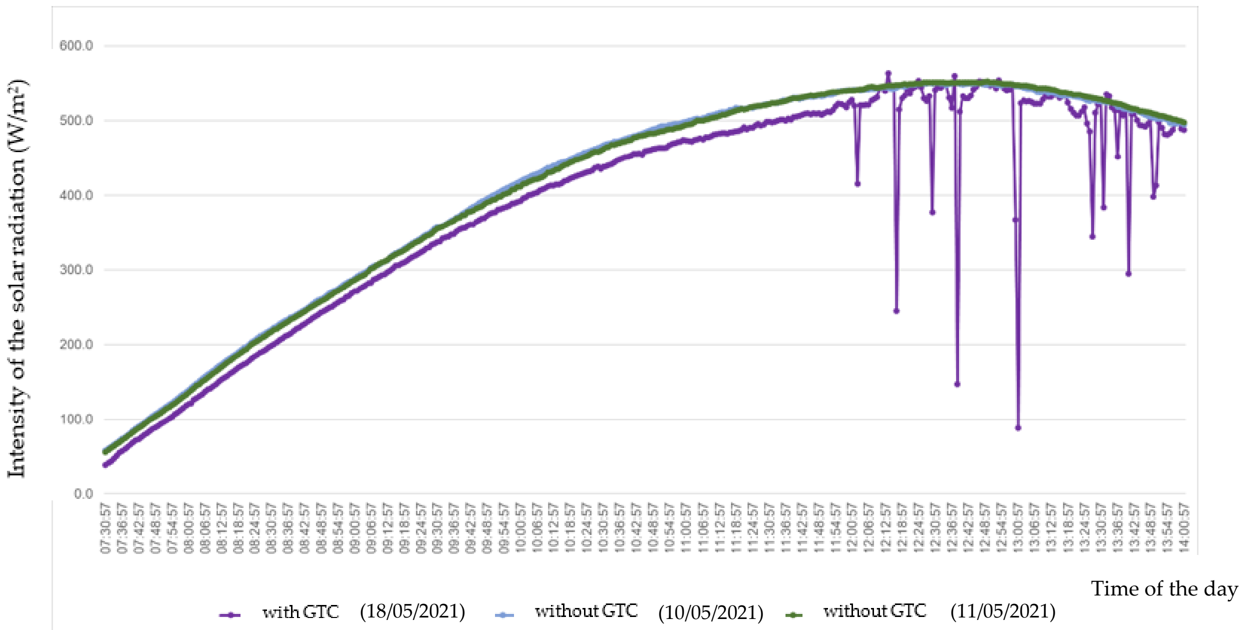

Figure 13. Days chosen for analysis: solar radiation intensity.

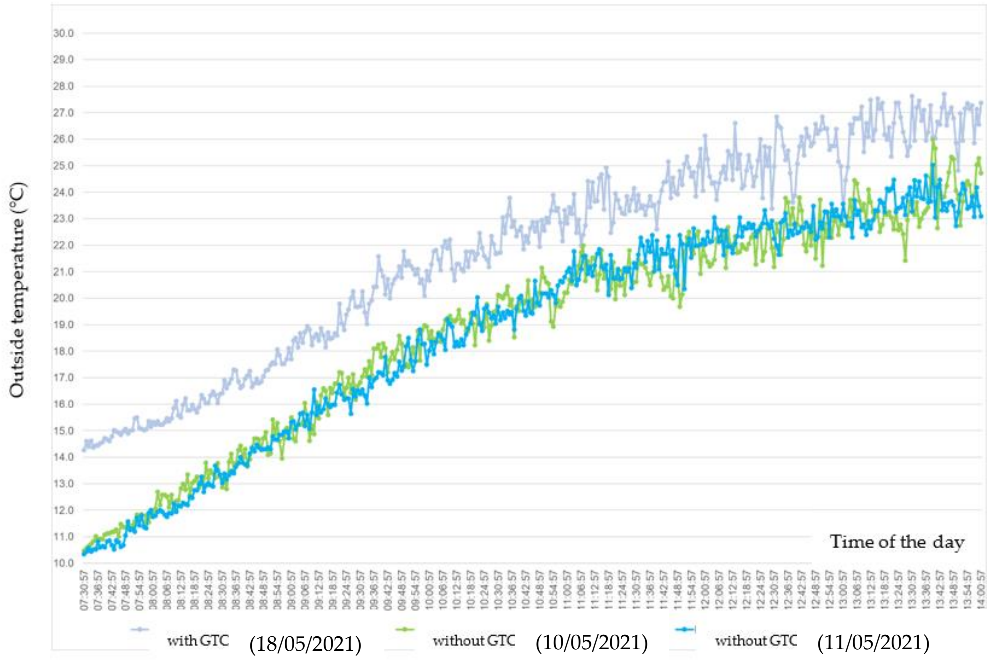

Figure 14. Days chosen for analysis: outside temperature.

In addition, we present the mean values of the solar radiation and outdoor temperature for these days throughout the experiments in Table 7.

Table 7. Days chosen for analysis: weather data (average values).

Parameter/Configuration (Day)	Without GTC (10 May 2021)	Without GTC (11 May 2021)	With GTC (18 May 2021)
ambient temperature (°C)	18.9	18.8	21.8
solar radiation intensity (W/m^2)	411	410	387

- GTC energy-saving assessment:

In order to evaluate the GTC contribution to the energy saving of the experimental building, the following situations were analyzed: the energy required to heat the container using the air conditioner in heat pump mode (indoor temperature set-point: 22 °C), while the fresh air required for ventilation was supplied through the GTC or directly from outside. The results achieved for the three days mentioned above (without/with GTC) are shown in Table 8.

Table 8. Heating energy consumption: experimental building without/with GTC.

Energy Consumption/Configuration (Day)	Without GTC (10 May 2021)	Without GTC (11 May 2021)	With GTC (18 May 2021)
Container heating (kWh)	1.12	1.23	0.94

It can be seen from the data in Table 8 that the energy savings due to preheating the ventilation air through the GTC were between 16 and 23% although the absolute difference in energy consumption seems very low (below 0.3 kWh).

Furthermore, based on the experimental results concerning the air temperature rise through the GTC (installed on the façade of the container), the reduction in container ventilation load due to the GTC was determined for several days. This evaluation is based on the following expression:

$$Q = V\rho c_p\left(T_{set-point} - T_{air}\right) \tag{3}$$

where V—ventilation airflow rate (m^3/s); ρ—air density (kg/m^3); c_p—air specific heat capacity (J/kg/°C); $T_{set\text{-}point}$ = container indoor temperature (°C); and T_{air}—ventilation (supply) air temperature (°C).

The values used in Equation (3) are: ventilation airflow rate, 0.02 m^3/s (72 m^3/h as explained before); container indoor temperature, 22 °C (temperature set-point). On the other hand, the supply air temperature is either the GTC outlet air temperature or outdoor temperature, depending on whether or not the air is passing through the GTC. Consequently, the values of the ventilation air temperature in Equation (3) are, according to Table 9, dependent on the configuration (without/with GTC). In fact, the temperature without the GTC (Table 9) is the measured mean GTC air inlet temperature (corresponding to the ambient temperature) and the temperature with the GTC (Table 9) is the measured mean GTC outlet air temperature.

Table 9. Ventilation (supply) air temperature without/with GTC.

Hour/Configuration (Day) Temperature (°C)	Without/With GTC (15 April 2021)	Without/With GTC (16 April 2021)	Without/With GTC (21 April 2021)	Without/With GTC (18 May 2021)
8	7.3/9.4	6.5/9.3	11/12.2	16.5/17.7
9	8.4/11	9.7/18.1	14.1/21.0	19.8/23.9
10	9.3/12.4	12.5/27.0	16.7/26.8	22.2/30.2
11	11.9/17.2	13.8/28.1	17.8/28.9	23.9/34.5
12	15.1/25	17.6/35.6	21.0/35.5	25.3/37.0
13	17.1/30.7	17.6/33.7	19.5/30.3	26.6/37.4

In addition, the ventilation load calculation for air heating, according to Equation (3), is only completed for situations where the outside temperature or GTC outlet air temperature is lower than the building indoor temperature set-point (22 °C).

The results for the hourly ventilation load to heat the air up to the temperature set-point without/with GTC are given in Table 10.

Table 10. Experimental building ventilation load without/with GTC.

Hour/Configuration (Day) Ventilation Load (W)	Without/With GTC (15 April 2021)	Without/With GTC (16 April 2021)	Without/With GTC (21 April 2021)	Without/With GTC (18 May 2021)
8	354/304	374/306	265/236	133/104
9	328/265	296/94	190/24	53/-
10	306/231	229/-	128/-	-/-
11	243/116	198/-	101/-	-/-
12	166/-	106/-	24/-	-/-
13	118/-	106/-	60/-	-/-

According to Table 10, the ventilation load reductions, due to the GTC integration in the container ventilation system, varied from 10% to almost 90%, depending on the weather conditions. Deeper analysis shows that for solar radiation below 200 W/m^2, the GTC contribution to reduce the ventilation load was only 10–25%, regardless of whether the outside temperature was lower or higher. On the other hand, solar radiation values between 250 and 380 W/m^2 led to important cutbacks in the ventilation load, generally over 50%, reaching sometimes 90%, even if the outside air temperature was relatively low. Finally, for solar radiation intensities over 400 W/m^2, the GTC outlet air temperature exceeded the considered interior temperature set-point of 22 °C.

3. Conclusions

The main objective of this work was to optimize the design of a glazed transpired solar collector (GTC) and to assess its potential in reducing the energy consumption of buildings when it is integrated in ventilation systems. The investigations were entirely based on experimental studies. The experimental tests indicated that the GTC design with 30 mm between the absorber and the glass layer leads to enhanced heat transfer effectiveness and overall efficiency regardless of airflow rates. This configuration of the GTC prototype was installed within the façade of a full-scale experimental building. The results, based on long-term analysis, showed that the energy consumption for heating and ventilation was substantially reduced in the case of the building with the GTC compared to the configuration without the GTC. The savings in terms of ventilation load can reach 90%, depending on solar radiation. Moreover, the ventilation load reductions can be up to 25% even under unfavorable weather conditions (reduced solar radiation intensity and low outside temperature).

These data confirm the significant capacity of GTCs to contribute to the overall energy performance of buildings, especially in cold and windy climates. This is all the more important as the recent coronavirus pandemic led to higher demands concerning the minimum rates of outdoor air ventilation in buildings. In this context, solar air-heating applications, especially those based on GTCs which can be wider and less restricted by climate conditions, represent proper solutions to minimize this increased energy demand of ventilation.

However, the technology based on solar air collectors (including GTCs), despite some progress, remains underutilized compared to its huge potential. Consequently, further analyses should be performed, together with numerical modeling, to continuously improve the efficiency of this equipment and its integration within the facades of buildings and ventilation systems.

As a result, this study should be further considered to investigate innovative designs of GTCs (e.g., with embodied phase-changing materials) under different climate scenarios and various thermal inertia characteristics of buildings.

Author Contributions: Conceptualization, C.I.T. and C.S.; methodology, C.I.T., C.S. and F.B.; validation, C.I.T. and F.B.; formal analysis, C.I.T. and C.S.; investigation, C.S. and C.C.; data curation, C.S. and C.C.; writing—original draft preparation, C.I.T.; writing—review and editing, C.I.T. and C.C.; visualization, C.I.T.; supervision, C.I.T.; project administration, C.C.; funding acquisition, C.C. All authors have read and agreed to the published version of the manuscript.

Funding: This research was funded by the Executive Agency for Higher Education, Research, Development and Innovation Funding (UEFISCDI), "Building integrated solar crop dryer for food preservation in urban farming applications (BISCUIT)"—grant number PN-III-P2-2.1-PED-2019-4165 and "Adaptive air solar collector with integrated nano-enhanced phase changing materials"—grant number PN-III-P2-2.1-PED-2021-1903. The APC was funded by the INSTRUCT 5-CNFIS-FDI-2022-0397 project.

Institutional Review Board Statement: Not applicable.

Informed Consent Statement: Not applicable.

Conflicts of Interest: The authors declare no conflict of interest.

References

1. Energy Prices: Commission Proposes Emergency Market Intervention to Reduce Bills for Europeans—Press Release 14 September 2022, Brussels. Available online: https://ec.europa.eu/commission/presscorner/detail/en/IP_22_5489 (accessed on 5 October 2022).
2. European Union. Directive 2009/28/EC of the European Parliament and of the Council of 23 April 2009 on the promotion of the use of energy from renewable sources and amending and subsequently repealing Directives 2001/77/EC and 2003/30/EC. *Off. J. Eur. Union* **2009**, *140*, 16–62.
3. European Union. Directive (EU) 2018/2001 of the European Parliament and of the Council of 11 December 2018 on the promotion of the use of energy from renewable sources. *Off. J. Eur. Union* **2018**, *328*, 82–209.
4. European Environment Agency. Share of Energy Consumption from Renewable Sources in Europe. Available online: https://www.eea.europa.eu/ims/share-of-energy-consumption-from (accessed on 27 October 2022).
5. Moschella, M.; Tucci, M.; Crisostomi, E.; Betti, A. A Machine Learning Model for Long-Term Power Generation Forecasting at Bidding Zone Level. In Proceedings of the 2019 IEEE Pes Innovative Smart Grid Technologies Europe (ISGT-Europe) Conference, Bucharest, Romania, 29 September–2 October 2019.

6. Ceglia, F.; Marrasso, E.; Roselli, C.; Sasso, M. Time-evolution and forecasting of environmental and energy performance of electricity production system at national and at bidding zone level. *Energy Convers. Manag.* **2022**, *265*, 115772. [CrossRef]
7. Pfeifer, A.; Herc, L.; Bjelic, I.B.; Duic, N. Flexibility index and decreasing the costs in energy systems with high share of renewable energy. *Energy Convers. Manag.* **2021**, *240*, 114258. [CrossRef]
8. Gaspari, M.; Lorenzoni, A. The governance for distributed energy resources in the Italian electricity market: A driver for innovation? *Renew. Sustain. Energy Rev.* **2018**, *82*, 3623–3632. [CrossRef]
9. Winkler, J.; Gaio, A.; Pfluger, B.; Ragwitz, M. Impact of renewables on electricity markets—Do support schemes matter? *Energy Policy* **2016**, *93*, 157–167. [CrossRef]
10. Ceglia, F.; Marrasso, E.; Roselli, C.; Sasso, M. An innovative environmental parameter: Expanded Total Equivalent Warming Impact (Un paramètre environnemental innovant: Impact de réchauffement total équivalent étendu). *Int. J. Refrig.* **2021**, *131*, 980–989. [CrossRef]
11. 2021 Global Status Report for Buildings and Construction. Available online: https://globalabc.org/resources/publications/2021-global-status-report-buildings-and-construction (accessed on 6 October 2022).
12. Weiss, W.; Spörk-Dür, M. Global Market Development and Trends in 2021. In *Solar Heat Worldwide*, 2022th ed.; Detailed Market Figures 2020; AEE—Institute for Sustainable Technologies: Gleisdorf, Austria, 2022; pp. 8–32.
13. Reichl, C.; Kramer, K.; Thoma, C.; Benovsky, P.; Lemee, T. Comparison of modelled heat transfer and fluid dynamics of a flat plate solar air heating collector towards experimental data. *Sol. Energy* **2015**, *120*, 450–463. [CrossRef]
14. Paya-Marin, M.A. Chapter 5—Solar Air Collectors for Cost-Effective Energy-Efficient Retrofitting. In *Cost-Effective Energy Efficient Building Retrofitting*; Woodhead Publishing: Cambridge, UK, 2017; pp. 141–168.
15. Goyal, R.K.; Tiwari, G.N.; Garg, H.P. Effect of thermal storage on the performance of an air collector: A periodic analysis. *Energy Convers. Manag.* **1998**, *39*, 193–202. [CrossRef]
16. Leon, M.A.; Kumar, S. Mathematical modeling and thermal performance analysis of unglazed transpired solar collectors. *Sol. Energy* **2007**, *81*, 62–75. [CrossRef]
17. Budea, S. Solar Air Collectors for Space Heating and Ventilation Applications—Performance and Case Studies under Romanian Climatic Conditions. *Energies* **2014**, *7*, 3781–3792. [CrossRef]
18. Wang, X.L.; Bo, L.; Bi, H.Q.; Yu, T. A simplified method for evaluating thermal performance of unglazed transpired solar collectors under steady state. *Appl. Therm. Eng.* **2017**, *117*, 185–192. [CrossRef]
19. Gunnewiek, L.H.; Hollands, K.G.T.; Brundrett, E. Effect of wind on flow distribution in unglazed transpired-plate collectors. *Sol. Energy* **2002**, *72*, 317–325. [CrossRef]
20. Bal, L.M.; Satya, S.; Naik, S.N. Solar dryer with thermal energy storage systems for drying agricultural food products: A review. *Renew. Sustain. Energy Rev.* **2010**, *14*, 2298–2314. [CrossRef]
21. Shukla, A.; Nkwetta, D.N.; Cho, Y.J.; Stevenson, V.; Jones, P. A state of art review on the performance of transpired solar collector. *Renew. Sustain. Energy Rev.* **2012**, *16*, 3975–3985. [CrossRef]
22. Mund, C.; Rathore, S.K.; Sahoo, R.K. A review of solar air collectors about various modifications for performance enhancement. *Sol. Energy* **2021**, *228*, 140–167. [CrossRef]
23. Kenna, J.P. The thermal trap solar collector. *Sol. Energy* **1983**, *31*, 335–338. [CrossRef]
24. Cordeau, S.; Barrington, S. Performance of unglazed solar ventilation air pre-heaters for broiler barns. *Sol. Energy* **2011**, *85*, 1418–1429. [CrossRef]
25. Chan, H.Y.; Zhu, J.; Ruslan, M.H.; Sopian, K.; Riffat, S. Thermal analysis of flat and transpired solar facades. *Energy Procedia* **2014**, *48*, 1345–1354. [CrossRef]
26. Belusko, M.; Saman, W.; Bruno, F. Performance of jet impingement in unglazed air collectors. *Sol. Energy* **2008**, *82*, 389–398. [CrossRef]
27. Brown, C.; Perisoglou, E.; Hall, R.; Stevenson, V. Transpired Solar Collector Installations in Wales and England. *Energy Procedia* **2014**, *48*, 18–27. [CrossRef]
28. Peci, F.; Taboas, F.; Comino, F.; de Adana, M.R. Experimental study of a modular Unglazed transpired collector Façade for building refurbishment. *Sol. Energy* **2020**, *201*, 247–258. [CrossRef]
29. Li, X.L.; Zheng, S.J.; Tian, G.; Zhang, L.; Yao, W.X. A new energy saving ventilation system assisted by transpired solar air collectors for primary and secondary school classrooms in winter. *Build. Environ.* **2020**, *177*, 106895. [CrossRef]
30. Tajdaran, S.; Kendrick, C.; Hopkins, E.; Bonatesta, F. Geometrical optimisation of Transpired Solar Collectors using design of experiments and computational fluid dynamics. *Sol. Energy* **2020**, *197*, 527–537. [CrossRef]
31. Collins, M.R.; Abulkhair, H. An evaluation of heat transfer and effectiveness for unglazed transpired solar air heaters. *Sol. Energy* **2014**, *99*, 231–245. [CrossRef]
32. Konttinen, P.; Salo, T.; Lund, P.D. Degradation of unglazed rough graphite-aluminium solar absorber surfaces in simulated acid and neutral rain. *Sol. Energy* **2005**, *78*, 41–48. [CrossRef]
33. Gao, L.X.; Bai, H.; Mao, S.F. Potential application of glazed transpired collectors to space heating in cold climates. *Energy Convers. Manag.* **2014**, *77*, 690–699. [CrossRef]
34. Zheng, W.D.; Li, B.J.; Zhang, H.; You, S.J.; Li, Y.; Ye, T.Z. Thermal characteristics of a glazed transpired solar collector with perforating corrugated plate in cold regions. *Energy* **2016**, *109*, 781–790. [CrossRef]

35. Gao, M.; Fan, J.H.; Furbo, S.; Xiang, Y.T. Energy and exergy analysis of a glazed solar preheating collector wall with non-uniform perforated corrugated plate. *Renew. Energy* **2022**, *196*, 1048–1063. [CrossRef]
36. Zhang, T.T.; Tan, Y.F.; Zhang, X.D.; Li, Z.G. A glazed transpired solar wall system for improving indoor environment of rural buildings in northeast China. *Build. Environ.* **2016**, *98*, 158–179. [CrossRef]
37. Nahar, N.M.; Garg, H.P. Free convection and shading due to gap spacing between an absorber plate and the cover glazing in solar energy flat-plate collectors. *Appl. Energy* **1980**, *7*, 129–145. [CrossRef]
38. Charvat, P.; Klimes, L.; Pech, O. Experimental and numerical study into solar air collectors with integrated latent heat thermal storage. In Proceedings of the Conference on Central Europe towards Sustainable Building (CESB13), Prague, Czech Republic, 26–28 June 2013.
39. Karim, M.A.; Hawlader, M.N.A. Performance investigation of flat plate, v-corrugated and finned air collectors. *Energy* **2006**, *31*, 452–470. [CrossRef]
40. El-Sebaii, A.A.; Aboul-Enein, S.; Ramadan, M.R.I.; Shalaby, S.M.; Moharram, B.M. Thermal performance investigation of double pass-finned plate solar air heater. *Appl. Energy* **2011**, *88*, 1727–1739. [CrossRef]
41. El-Sebaii, A.A.; Aboul-Enein, S.; Ramadan, M.R.I.; Shalaby, S.M.; Moharram, B.M. Investigation of thermal performance of-double pass-flat and v-corrugated plate solar air heaters. *Energy* **2011**, *36*, 1076–1086. [CrossRef]
42. Chabane, F.; Moummi, N.; Benramache, S. Experimental study of heat transfer and thermal performance with longitudinal fins of solar air heater. *J. Adv. Res.* **2014**, *5*, 183–192. [CrossRef] [PubMed]
43. Ozgen, F.; Esen, M.; Esen, H. Experimental investigation of thermal performance of a double-flow solar air heater having aluminium cans. *Renew. Energy* **2009**, *34*, 2391–2398. [CrossRef]
44. Omojaro, A.P.; Aldabbagh, L.B.Y. Experimental performance of single and double pass solar air heater with fins and steel wire mesh as absorber. *Appl. Energy* **2010**, *87*, 3759–3765. [CrossRef]
45. El-khawajah, M.F.; Aldabbagh, L.B.Y.; Egelioglu, F. The effect of using transverse fins on a double pass flow solar air heater using wire mesh as an absorber. *Sol. Energy* **2011**, *85*, 1479–1487. [CrossRef]
46. Gao, M.; Wang, D.J.; Liu, Y.F.; Wang, Y.Y.; Zhou, Y. A study on thermal performance of a novel glazed transpired solar collector with perforating corrugated plate. *J. Clean. Prod.* **2020**, *257*, 120443. [CrossRef]
47. Croitoru, C.V.; Năstase, I.; Bode, F.I.; Meslem, A. Thermodynamic investigation on an innovative unglazed transpired solar collector. *Sol. Energy* **2016**, *131*, 21–29. [CrossRef]
48. Bejan, A.S.; Teodosiu, C.; Croitoru, C.V.; Catalina, T.; Năstase, I. Experimental investigation of transpired solar collectors with/without phase change materials. *Sol. Energy* **2021**, *214*, 478–490. [CrossRef]
49. Croitoru, C.; Bode, F.; Teodosiu, C.; Catalin, T.; Bejan, A.S. Experimental investigation of an enhanced transpired air solar collector with embodied phase changing materials. *J. Clean. Prod.* **2022**, *336*, 130398.
50. Berville, C.; Bode, F.; Croitoru, C. Numerical Simulation Investigation of a Double Skin Transpired Solar Air Collector. *Appl. Sci.* **2022**, *12*, 520. [CrossRef]
51. Bejan, A.S.; Labihi, A.; Croitoru, C.V.; Bode, F.; Sandu, M. Experimental Investigation of the Performance of a Transpired Solar Collector Acting as a Solar Wall. In Proceedings of the ISES Solar World Congress 2017, Abu Dhabi, United Arab Emirates, 29 October–2 November 2017.
52. Zhang, T.T.; Tan, Y.F.; Yang, H.X.; Zhang, X.D. The application of air layers in building envelopes: A review. *Appl. Energy* **2016**, *165*, 707–734. [CrossRef]
53. Van Decker, G.W.E.; Hollands, K.G.T.; Brunger, A.P. Heat-exchange relations for unglazed transpired solar collectors with circular holes on a square or triangular pitch. *Sol. Energy* **2001**, *71*, 33–45. [CrossRef]
54. Ferahta, F.Z.; Bougoul, S.; Médale, M.; Abid, C. Influence of the Air Gap Layer Thickness on Heat Transfer Between the Glass Cover and the Absorber of a Solar Collector. *Fluid Dyn. Mater. Process.* **2012**, *8*, 339–351.
55. Taylor, J.R. *An Introduction to Error Analysis—The Study of Uncertainties in Physical Measurements*, 2nd ed.; University Science Books: Sausalito, CA, USA, 1997; pp. 45–92.
56. American Society of Heating, Refrigerating and Air-Conditioning Engineers. *ANSI/ASHRAE Standard 62.1-2022, Ventilation and Acceptable Indoor Air Quality*, 2022th ed.; ASHRAE: Peachtree Corners, GA, USA, 2022.